International Journal of Fracture (2005) 131:59–78
DOI 10.1007/s10704-004-3638-4

Fatigue limit reliability of axisymmetric complex surface

YUUTA AONO* and HIROSHI NOGUCHI
Faculty of Engineering, Kyushu University, 6-10-1 Hakozaki, Higashi-ku, Fukuoka, 812-8581, Japan. Phone: 81-92-642-3375
**Author for correspondence (E-mails: aono@mech.kyushu-u.ac.jp; nogu@mech.kyushu-u.ac.jp)*

Received 8 June 2004; accepted in revised form 15 September 2004

Abstract. In this paper, a method to predict fatigue limit reliability of specimens with 2D complex rough surface is proposed. First, a effective surface profile on fatigue limit is proposed. This is obtained from the ineffective crack length against the fatigue limit. Next, an equivalent notch depth is proposed to replace a rough profile to a smooth profile with a notch. To calculate the stress concentration of the notch and to determine the equivalent notch depth, an exact solution is given for a problem of an infinite plate with a complex profile under tension. The solution is obtained with the complex variable method. Finally, a method to predict the fatigue limit reliability is discussed. The Linear Notch Mechanics and $\sqrt{\text{area}}$ parameter model is used to predict the fatigue limit of a smooth profile with a notch, and then the fatigue limit reliability is estimated with the fatigue limit of many simulated surfaces. Moreover, rotating bending fatigue tests of 0.1% carbon steel with a complex surface are carried out. The experimental fatigue limit data is compared with the present estimated value. As results, the validity of the present method is examined.

Key words: Fatigue limit, notch, reliability, stress concentration, surface roughness.

1. Introduction

An essential characteristic of metal fatigue is an uniqueness of phenomenon. Same fatigue behavior never reappear because of instability of slip behavior, scatter of microstructure and difference of surface texture on real structures. Therefore, metal fatigue characteristics consist of the material property and the surface texture.

Siebel and Gaier (1957) have done fatigue tests of steel and non-ferrous metal made from several kinds of production technique. They pointed out that fatigue limit does not change under the condition of $R_{\max} < 1\mu$m and fatigue limit reduction of larger $R_{\max}$ can be expressed as an unique function of $R_{\max}$ in some extent. Therefore the surface factor as the function of $R_{\max}$ or R_a have been used as the fundamental data for fatigue strength design. Surface factor is defined as the ratio of the fatigue limit with a real surface to that with an ideal surface, for example $R_{\max} < 1\mu$m. However the decision making of surface factor has a poor physical background and the scatter is large. As a result, safe factor are used by experience. Then as the most fundamental mechanical properties are vague, the reasonable design is confined.

On the other hand, the influences of surface texture on fatigue limit are classified by following three factors (Taylor and Clancy, 1991).

1. stress concentration due to surface configuration;
2. material property changing due to plastic deformation; dislocation structure, fine graining, amorphous.
3. residual stress due to plastic deformation or transformation.

As these factors are connected mutually, the effect of each factor cannot be measured or predicted exactly.

However the tendency of each factor is reported as a case-study. For example, El-Helieby and Rowe (1980) have done the fatigue tests of three types of cut high strength steel after stress relief annealing in order to notice the effect of surface roughness and residual stress, and then reported that the effect of residual stress is larger than that of surface roughness. Sinclair et al.(1957) have done the fatigue tests of various kinds of surface finished titanium alloy and reported that the effect of work hardening is larger than that of surface roughness.

About Factor 1, there are some analytical and quantitative studies. Taylor and Clancy (1991) made bainite steel with various $R_{\max}$ due to different finishings and did the fatigue tests after residual stress relief annealing. They pointed out that the effect of relatively lower roughness level can be considered as a small crack whose length is $R_{\max}$. On the other hands, the effect of higher roughness level should be considered as a notch. Andrews and Sehitoglu (2000) proposed the prediction method for fatigue life with two geometry parameters, notch depth (= the distance from the average line to the valley root) and notch root radius, considering crack closure phenomenon.

On the other hand, authors think that Factor 1 influences the fatigue limit reliability and Factors 2 and 3 influence the average fatigue limit characteristics. In this paper, the effect of Factor 1 is discussed. The difficulty of analyzing the effect of complex surface configuration are as follows:

1. Stress analysis can not be carried out on each surface of real structures. Each surface profile is unique because of the geometrical non-reappearbility.
2. Even if the stress states are found, fatigue limit can not be predicted quantitatively. Because there is not an expression for a quantitative evaluation of fatigue limit for an arbitrary small notch and crack.

A simple formula for Problem 2 was proposed recently by the present authors (Miyazaki et al., 2004). In this paper, a 2D stress analysis method of a certain complex surface profile is discussed and a computational simulation of a rough surface is also proposed to solve Problem 1.

A diagram to predict a fatigue limit reliability is shown in Figure 1. As surface roughness is generally irregular, the fatigue limit of specimen with a roughness has a scatter. Therefore, in this paper, the fatigue limit reliability is estimated from the meso-characteristics as shown in Figure 1.

In order to express the irregularity of roughness, many similar roughness are reproduced by a computational simulation from a measured roughness; by this procedure, many experiments become unnecessary. This procedure will be described in Section 2.

Each simulated roughness on computer is cut off trivial elements of roughness wave not to influence the fatigue characteristic of the material. This cut off profile is called the effective profile on fatigue limit. Moreover the profile is transformed to a notch or a crack; this procedure will be described in Section 3. In this transformation process, stress concentration factors(SCF) in an effective profile on fatigue limit is required. In Section 4, an elastic solution of complex profile is obtained to calculate the SCF.

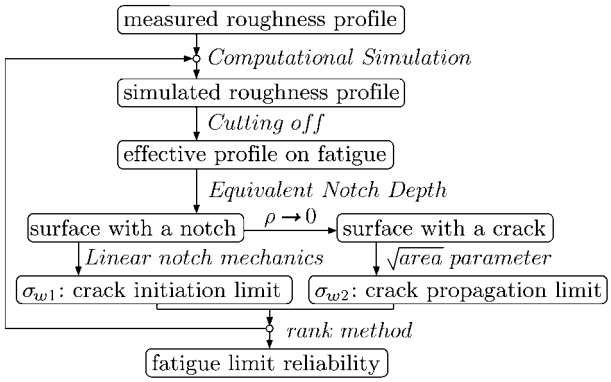

Figure 1. Diagram to evaluate fatigue limit reliability.

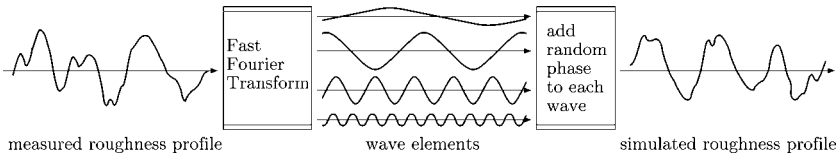

Figure 2. Roughness profile simulation.

The prediction method of fatigue limit reliability is described in Section 5. The fatigue limit of each simulated surface profile is evaluated to obtain the reliability. In Section 6, the limitation of the present method is examined in the view of the characteristics of surface profile.

Finally, in Section 7, an application to an axisymmetric surface roughness is shown.

2. Simulation of roughness

If a surface profile is regarded as a stochastic process, it is well known that the profile can be simulated by a computational method such as spectrum analysis.

In this paper, surface profiles are assumed to be stationary stochastic process. Then as Figure 2 shows, spectrum analysis with FFT is carried out on a measured surface profile, and a random phase is added to each wave element to obtain a simulated profile with the Inverse FFT.

As it is mentioned above, stationary stochastic process is assumed in this paper. Unless the characteristic of roughness profile is governed by stationary stochastic process, another appropriate computational method should be applied.

3. Transformation from roughness to a notch and a crack

NOMENCLATURE

$\sqrt{\text{area}}$	square root of projected area of a defect perpendicular to the first principal stress
$\sqrt{\text{area}}_{\text{min}}$	minimum defect size effective on fatigue limit

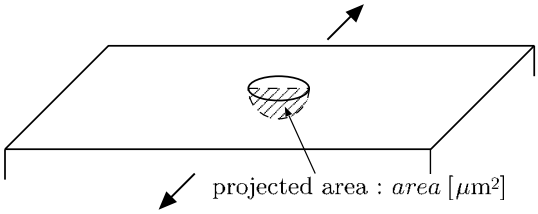

Figure 3. Definition of $\sqrt{\text{area}}$ parameter.

c	crack length
$c_{\min}$	minimum crack length effective on fatigue limit
H_V	Vicker's hardness
K_t	stress concentration factor
$R_{\max}$	maximum height of a surface profile
R_a	mean deviation of a surface profile
$R(x)$	measured roughness profile
t	notch depth
$W(x)$	effective profile on fatigue limit
σ_{w0}	fatigue limit of plain surface
σ_{w1}	fatigue crack initiation limit
σ_{w2}	fatigue crack propagation limit
ρ	notch root radius

3.1. Effective profile on fatigue limit

Siebel showed that the critical value of $R_{\max}$ which influences on fatigue limit exists.

Hardness, H_B or H_V, have strong correlation with fatigue limit (Garwood et al., 1951). Here, a fatigue limit of a plain specimen is denoted σ_{w0} and is expressed with Vickers hardness H_V under the condition of the stress ratio $R=-1$ by following equation empirically (Murakami, 2002).

$$\sigma_{w0} = 1.6H_V. \tag{1}$$

While crack propagation limit of a specimen with a defect as shown in Figure 3 is denoted σ_{w2} and can be expressed with the projected area area(μm^2) of the defect perpendicular to the first principal stress and H_V under the condition of the stress ratio $R=-1$ (Murakami, 2002)

$$\sigma_{w2}(\sqrt{\text{area}}) = \frac{1.43(H_V+120)}{\sqrt{\text{area}}^{1/6}}. \tag{2}$$

The minimum defects size effective on fatigue limit, $\sqrt{\text{area}}_{\min}(\mu\text{m})$, can be expressed as the intersection point between Eqs. (1) and (2) as follows:

$$\sqrt{\text{area}}_{\min} = \left[\frac{1.43(H_V+120)}{1.6H_V}\right]^6. \tag{3}$$

The effective profile on fatigue limit is defined as a coarse grained line, neglected the roughness ineffective on fatigue limit Fig 4. Namely, when the roughness curve

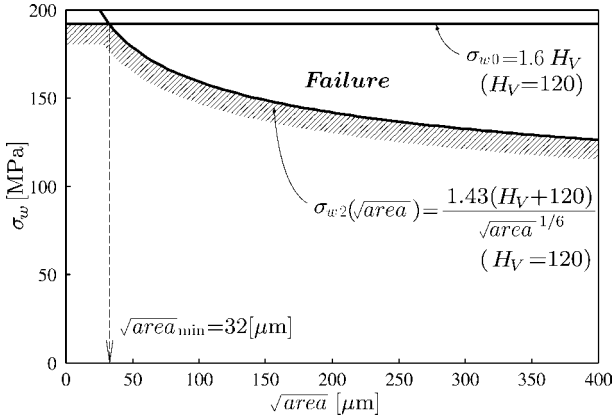

Figure 4. Ineffective $\sqrt{\text{area}}$ parameter on fatigue limit in the case of $H_V = 120$.

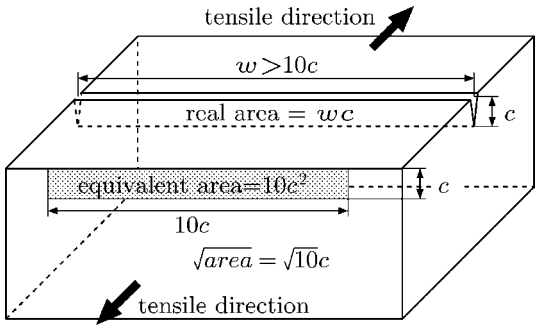

Figure 5. Equivalent $\sqrt{\text{area}}$ parameter for 2D crack.

and the effective profile are denoted with $R(x)$ and $W(x)$, respectively, then $W(x)$ is given by Eq (4).

$$|R(x) - W(x)| < c_{\min}, \tag{4}$$

where $c_{\min}$ is the length of 2D crack which corresponds to $\sqrt{\text{area}}_{\min}$ under the same K value as shown in Figure 5. The transformation from $\sqrt{\text{area}}_{\min}$ to $c_{\min}$ is expressed by the following equation (Murakami, 1985):

$$c_{\min} = \frac{\sqrt{\text{area}}_{\min}}{\sqrt{10}}. \tag{5}$$

Namely, the effective profile on fatigue limit is obtained by removing high frequency wave elements to satisfy the condition of Eq. (4).

3.2. Equivalent notch depth

In this section, the method to transform from the effective profile on fatigue limit to the equivalent smooth profile with a notch or a crack is discussed.

As an effective profile on fatigue limit has a complex configuration, interaction effect should be considered in order to estimate stress concentration; this effect is important.

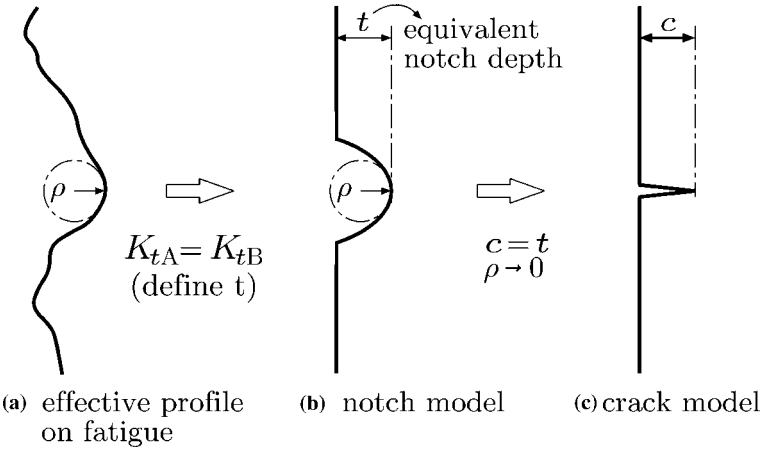

Figure 6. Evaluation of notch depth and crack length: (a) effective profile on fatigue; (b) notch model; (c) Crack model on fatigue.

In the case of 2D problem, an elastic stress analysis of a complex surface profile is proposed in Section 4. If a stress concentration factor K_t is obtained, an equivalent notch depth can be defined as shown in Figure 6. 6a shows an effective profile on fatigue limit. After a stress concentration factor K_{tA} is obtained, an equivalent notch depth can be estimated by the condition of $K_{tA} = K_{tB}$ and the equivalent ellipse concept (Inglis, 1913); K_{tB} is a stress concentration factor of a plate with a semi-elliptical notch. Namely, the equivalent notch depth t is calculated by Eq. (6)

$$t = \left(\frac{K_{tA} - 1}{2}\right)^2 \rho. \tag{6}$$

Thus an effective profile on fatigue limit is transformed to a profile with an elliptical notch, which has an equivalent depth t and a notch root radius ρ.

On the other hand, an equivalent crack length c is easily defined by an equivalent notch depth t and $\sqrt{\text{area}}$ parameter model (Murakami, 2002). As shown in Figure 6b and 6c, the notch depth t and the crack length c are equivalent, because the projected areas of the notch and crack are same. Therefore, the c value is equal to the t value.

4. Elastic stress analysis of an infinite plate with a complex surface profile

In this section, a 2D elastic solution and method to calculate stress concentration of an effective profile $W(x)$ on fatigue limit are described.

Nomenclature

A	a constant of Hirano's conformal mapping function about stress state at infinity
a	a positive parameter of Hirano's conformal mapping function
C_j	jth wave parameter of Hirano's conformal mapping function $(n = 1, 2, \ldots, n)$

$F(\lambda)$	negative boundary stress on the traction free boundary
$g_1(\zeta), g_2(\zeta)$	complex stress function on mapped plane about periodic stress state
$h(a)$	function of a which represent residual of the least square method
j	positive integer which represents number of Hirano's wave
k	maximum number of Hirano's wave
L	symbol of free surface boundary $\xi = 0$
$m(\zeta)$	Hirano's conformal mapping function
$P(\zeta)$	additional function of Plemelj solution
$\|r\|_2$	residual of the least square method
S^+, S^-	regions of $\xi > 0$ and $\xi < 0$, observed and auxiliary regions
x_0	translation of x-axis
x_n, y_n	data of points of surface profile $(n = 1, 2, \ldots)$
$z = x + iy$	physical coordinate
$\Phi(\zeta)$	Plemelj function
$\Phi^+(\zeta), \Phi^-(\zeta)$	Plemelj functions in regions $\xi > 0$ and $\xi < 0$
$\Psi(\zeta), \psi(\zeta)$	complex stress function on mapped plane
$\Psi_0(\zeta), \psi_0(\zeta)$	complex stress function on mapped plane about uniform stress state
λ	complex variable which stand for boundary
ρ	notch root radius
$\sigma_{\xi\xi}, \sigma_{\eta\eta}, \sigma_{\xi\eta}$	stresses in mapped coordinate
σ_∞	tensile stress at infinity
ω	parameter of period of Hirano's conformal mapping function
η_n	data of points on free surface boundary in the mapped plane $(n = 1, 2, \ldots)$
$\zeta = \xi + i\eta$	mapped coordinate

4.1. Mapping function for a complex surface profile

It is impossible to analyze an infinite plate with a real complex surface profile. Therefore in this paper, as shown in Figure 7a, it is assumed that a complex profile can be expressed as a finite length and the length is repeated periodically. The complex profile in a finite length can be expressed by developing the Hirano's conformal mapping function (Hirano, 1950). The mapping function is used in a 2D elastic solution derived later. The solution is a half infinite plate subjected to uniform tension at infinity. The following expression is the Hirano's conformal mapping function:

$$z = m(\zeta) = \zeta - \frac{\omega}{2} \sum_{j=1}^{k} C_j \coth \frac{j\omega}{2}(\zeta + a). \tag{7}$$

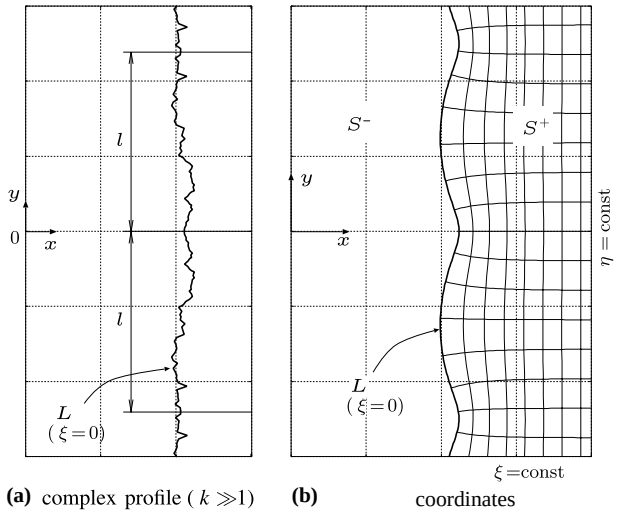

Figure 7. Symbols for the Hirano's conformal mapping: (a) complex profile ($k \gg 1$); (b) coordinates.

The physical and mapped coordinates are expressed as $z = x + iy$ and $\zeta = \xi + i\eta$, respectively. Here, ω is a real constant concerned with a period. C_j and a are real constants which are parameters for a configuration of a complex profile. a is positive. The periodic notch boundary can be expressed as $\xi = 0$ in Eq. (7) as shown in Figure 7b. Irregularity of a surface profile within a period can be obtained to increase k value and to be given proper C_j values.

4.2. Derivation of the solution

The boundary condition is formulated as the Hilbert's problem and the solution is derived by the complex variable method (England, 1971). At first, the stress field is expressed as the following complex functions $\Psi(\zeta)$ and $\psi(\zeta)$.

$$\sigma_{\xi\xi} + \sigma_{\eta\eta} = 2\left\{\Psi(\zeta) + \overline{\Psi(\zeta)}\right\}, \tag{8}$$

$$\sigma_{\xi\xi} - \sigma_{\eta\eta} + 2i\sigma_{\xi\eta} = -2\left\{\frac{m(\zeta)}{m'(\zeta)}\overline{\Psi'(\zeta)} + \frac{\overline{m'(\zeta)}}{m'(\zeta)}\overline{\psi(\zeta)}\right\}, \tag{9}$$

$$\Psi(\zeta) = \Psi_0(\zeta) + g_1(\zeta), \tag{10}$$

$$\psi(\zeta) = \Psi_0(\zeta) + \frac{m(\zeta)}{m'(\zeta)}\Psi_0'(\zeta) + \psi_0(\zeta) + g_1(\zeta) + \frac{m(\zeta)}{m'(\zeta)}g_1'(\zeta) + g_2(\zeta). \tag{11}$$

Here,

$$\Psi_0(\zeta) = \psi_0(\zeta) = \frac{A}{m'(\zeta)}, \tag{12}$$

where A is a constant about the stress state at infinity and described in detail later.

Stress functions $\Psi(\zeta)$ and $\psi(\zeta)$ are given as a combination of uniform stress functions, $\Psi_0(\zeta)$ and $\psi_0(\zeta)$, and unknown additional functions, $g_1(\zeta)$ and $g_2(\zeta)$. If $\Psi(\zeta)$ and $\psi(\zeta)$ are expressed in Eq. (10) and (11), respectively, where $g_1(\zeta)$ and $g_2(\zeta)$ are

periodic functions concerned with η, the stress field is also periodic concerned with η (refer to Appendix A in detail).

The unknown functions $g_1(\zeta)$ and $g_2(\zeta)$ should be determined to satisfy the traction-free boundary condition on $\xi = 0$. The traction-free boundary condition, $\sigma_{\xi\xi} + i\sigma_{\xi\eta} = 0$, is given on the boundary $\zeta = \lambda$ by Eq. (13):

$$\Psi(\lambda) + \overline{\Psi(\lambda)} - \frac{m(\lambda)}{m'(\lambda)}\overline{\Psi'(\lambda)} - \frac{\overline{m'(\lambda)}}{m'(\lambda)}\overline{\psi(\lambda)} = 0. \tag{13}$$

Equations (10) and (11) are substituted for the above equation in the mirror region $\zeta = -\overline{\zeta}$. Thus the boundary condition is formulated by Eq. (14):

$$\begin{aligned} &g_1(\lambda) + \left\{1 - \frac{\overline{m'(-\overline{\lambda})}}{m'(\lambda)}\right\}\overline{g_1(\lambda)} \\ &\quad - \frac{m(\lambda) + \overline{m(-\overline{\lambda})}}{m'(\lambda)}\overline{g_1'(-\overline{\lambda})} - \frac{\overline{m'(-\overline{\lambda})}}{m'(\lambda)}\overline{g_2(-\overline{\lambda})} = F(\lambda). \end{aligned} \tag{14}$$

Here, $F(\lambda)$ is the stresses on the traction-free boundary due to the remote stress at infinity and expressed by Eq. (15):

$$\begin{aligned} F(\lambda) &= -\Psi_0(\lambda) - \left\{1 - \frac{\overline{m'(-\overline{\lambda})}}{m'(\lambda)}\right\}\overline{\Psi_0(-\overline{\lambda})} \\ &\quad + \frac{m(\lambda) + \overline{m(-\overline{\lambda})}}{m'(\lambda)}\overline{\Psi_0'(-\overline{\lambda})} + \frac{\overline{m'(-\overline{\lambda})}}{m'(\lambda)}\overline{\psi_0(-\overline{\lambda})} \\ &= \frac{A}{m'(\lambda)} - \frac{A}{\overline{m'(-\overline{\lambda})}} - A\frac{m(\lambda) + \overline{m(-\overline{\lambda})}}{m'(\lambda)}\frac{\overline{m''(-\overline{\lambda})}}{\overline{m'(-\overline{\lambda})}^2}. \end{aligned} \tag{15}$$

Next, the following function $\Phi(\zeta)$ is defined to solve Eq. (14):

$$\Phi(\zeta) = \begin{cases} g_1(\zeta) & \text{for } \zeta \in S^+, \\ -\left\{1 - \dfrac{\overline{m'(-\overline{\lambda})}}{m'(\lambda)}\right\}\overline{g_1(-\overline{\lambda})} & \\ \quad + \dfrac{m(\lambda) + \overline{m(-\overline{\lambda})}}{m'(\lambda)}\overline{g_1'(-\overline{\lambda})} + \dfrac{\overline{m'(-\overline{\lambda})}}{m'(\lambda)}\overline{g_2(-\overline{\lambda})} & \text{for } \zeta \in S^-. \end{cases} \tag{16}$$

Here, S^+ and S^- represent the regions of $\xi > 0$ and $\xi < 0$, respectively. Equation (14) can be rewritten with the above function $\Phi(\zeta)$.

$$\Phi^+(\lambda) - \Phi^-(\lambda) = F(\lambda). \tag{17}$$

Equation (17) is called Plemelj formula. The solution of Plemelj formula is well-known as follows:

$$\Phi(\zeta) = \frac{1}{2\pi i}\int_L \frac{F(\lambda)d\lambda}{\lambda - \zeta} + P(\zeta). \tag{18}$$

Here L expresses the free surface boundary. $P(\zeta)$ is polynomial in terms of ζ. After integration of $F(\lambda)$ in Eq. (18) is carried out, the following solutions can be obtained in each region.
For $\zeta \in S^+$

$$\Phi(\zeta) = A\left\{\frac{1}{m'(\zeta)} - 1\right\} \tag{19}$$

for $\zeta \in S^-$

$$\Phi(\zeta) = A\left\{\frac{1}{\overline{m'(-\bar{\zeta})}} + \frac{m(\zeta) - \overline{m(-\bar{\zeta})}}{m'(\zeta)}\frac{\overline{m''(-\bar{\zeta})}}{\overline{m'(-\bar{\zeta})}^2} - 1\right\}. \tag{20}$$

On the other hand, unknown $g_1(\zeta)$ and $g_2(\zeta)$ ($\zeta \in S^+$) are obtained by substituting Eq. (19) and (20) for Eq. (16)

$$g_1(\zeta) = A\left\{\frac{1}{m'(\zeta)} - 1\right\}, \tag{21}$$

$$g_2(\zeta) = A\left\{2\frac{\overline{m''(-\bar{\zeta})}}{m'(\zeta)^2} - 2\frac{\overline{m''(-\bar{\zeta})}}{m'(\zeta)} - \frac{1}{m'(\zeta)} + 2\frac{m(\zeta) + \overline{m(-\bar{\zeta})}}{m'(\zeta)}\frac{m''(\zeta)}{m'(\zeta)^2} + 1\right\}. \tag{22}$$

Equations (21) and (22) have periodicity concerned with η, and satisfy the traction-free boundary condition represented by Eq. (13). However, as the mapping functions $\overline{m(-\bar{\zeta})}$ and $\overline{m'(-\bar{\zeta})}$ have a singular point at $\zeta = a$ in the plate, the singularity should be eliminated. If $P(\zeta)$ in Eq. (18) is assumed as follows, the unfavorable singularity can be eliminated:

$$P(\zeta) = \frac{\sigma_\infty}{4}\left\{-\frac{1}{m'(a)} + 1\right\}. \tag{23}$$

The final forms of $g_1(\zeta)$ and $g_2(\zeta)$ are obtained with the above $P(\zeta)$ by the following equations:

$$g_1(\zeta) = A\left\{\frac{1}{m'(\zeta)} - \frac{1}{m'(a)}\right\}, \tag{24}$$

$$g_2(\zeta) = A\left[\left\{2\frac{\overline{m'(-\bar{\zeta})}}{m'(\zeta)} - 1\right\}\left\{\frac{1}{m'(\zeta)} - \frac{1}{m'(a)}\right\} + 2\frac{m(\zeta) + \overline{m(-\bar{\zeta})}}{m'(\zeta)}\frac{m''(\zeta)}{m'(\zeta)^2}\right]. \tag{25}$$

The constant A can be obtained from the stress at infinity, σ_∞.

$$A = \frac{\sigma_\infty}{8 - \dfrac{3}{m'(a)} - \dfrac{1}{\overline{m'(a)}}}. \tag{26}$$

4.3. Examples of analysis

Two examples are showed with the solution described in Section 4.2. In this section, stress concentration factor K_t means $\sigma_{\max}/\sigma_\infty$. $\sigma_{\max}$ is the tangential normal stress at the notch root.

Table 1. Stress concentration factor of periodic notch in Figure 8.

p/ρ	5.0	6.0	8.0	10.0	$\left(1+2\sqrt{\frac{R_{\max}}{\rho}}\right)$
K_t	2.0095	2.0341	2.0610	2.0745	2.414
ω	1.25664	1.04720	0.78540	0.62832	–
a	2.80077	2.02313	1.72195	1.62867	–
C_1	−6.71227	−1.95746	−1.14851	−0.96409	–

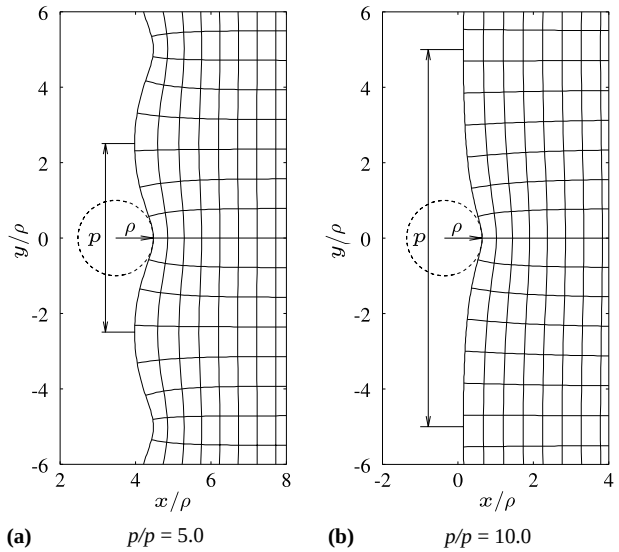

Figure 8. Periodic notch ($k=1$, $R_{\max}/\rho=0.5$): (a) $p/\rho=5.0$; (b) $p/\rho=10.0$.

The first examples are periodic notches for constant $R_{\max}/\rho = 0.5$ and various $p/\rho = 5, 6, 8, 10$ as shown in Figure 8. Here, p means a pitch of periodicity. These notches can be generated by three parameters, ω, a, and C_1. The stress concentrations are showed in Table 1 with the value by the equivalent ellipse concept (Inglis, 1913). K_t is larger as p/ρ increases. It gets closer to the value by the equivalent ellipse concept, but does not coincide even in the case of $p/\rho = 10$. The shape around notch root affects the stress concentration factor for relatively shallow notch, as in the case of $R_{\max}/\rho = 0.5$.

The second examples are periodic notches with the same pitch and different $R_{\max}/\rho$ as shown in Figure 9. The profiles are generated under $k=3$ and parameters are shown in Table 2 with K_t. K_t of Figure 9a and 9c are almost same, but notch root radius of these are different. Interference between notches cannot neglect in these cases. And it is supposed that real rough surface causes very complex interference.

4.4. Fitting of mapping function

The solution of a half infinite plate with complex surface was obtained in Section 4.3. But appropriate values of C_j and a are required to fit a real surface profile or an effective profile and to calculate stress concentrations of the profile.

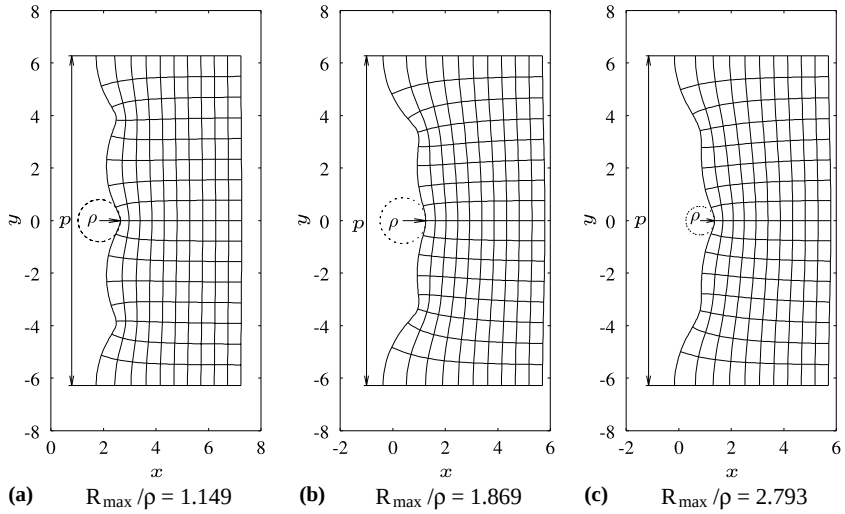

Figure 9. Periodic notch ($k=3, a=2.0, \omega=0.5, p=4\pi$): (a) $R_{\max}/\rho=1.149$; (b) $R_{\max}/\rho=1.869$; (c) $R_{\max}/\rho=2.793$.

Table 2. Stress concentration factor of Figure 9 ($k=3, a=2.0, \omega=0.5, p=4\pi$).

$R_{\max}/\rho$	1.149	1.869	2.793
K_t	2.8074	2.1646	2.7962
$1+2\sqrt{\frac{R_{\max}}{\rho}}$	3.1435	3.7343	4.3422
C_1	−1.0	−3.0	−5.0
C_2	2.0	7.0	5.0
C_3	−10	−7.0	−5.0

When data (x_n, y_n) $(n=1, 2, \ldots, n)$ are obtained from a surface profile, the following equations should be satisfied in order to fit it to the boundary $\xi=0$ of the mapping function.

$$x_n = -x_0 - \frac{\omega}{2}\sum_{j=1}^{k} C_j \frac{\sinh j\omega a}{\cosh j\omega a - \cos j\omega\eta_n}, \tag{27}$$

$$y_n = \eta_n + \frac{\omega}{2}\sum_{j=1}^{k} C_j \frac{\sin j\omega\eta_n}{\cosh j\omega a - \cos j\omega\eta_n}. \tag{28}$$

Here, x_0 is a translation of x-axis. Unknown parameters are x_0, C_j, a and η_n in the above Eq. (27) and (28). In this paper, these were determined by the following process:

1. At first, a proper initial value was given for a. Then C_j and x_0 were determined with the least square method. Initial values of η_n were given as $\eta_n = y_n$. The formulations of the least square method are represented by following equations:

$$\mathbf{FC} = \mathbf{x}, \tag{29}$$

$$\mathbf{F} = \begin{bmatrix} \left\{\frac{\partial f_x}{\partial C_1}\right\}_1 & \cdots & \left\{\frac{\partial f_x}{\partial C_k}\right\}_1 & \left\{\frac{\partial f_x}{\partial x_0}\right\}_1 \\ \vdots & \vdots & \vdots & \vdots \\ \left\{\frac{\partial f_x}{\partial C_1}\right\}_N & \cdots & \left\{\frac{\partial f_x}{\partial C_k}\right\}_N & \left\{\frac{\partial f_x}{\partial x_0}\right\}_N \end{bmatrix}, \tag{30}$$

$$\mathbf{C}^t = \begin{bmatrix} C_1 \cdots C_k \; x_0 \end{bmatrix}, \tag{31}$$

$$\mathbf{x}^t = \begin{bmatrix} x_1 \cdots x_N \end{bmatrix}, \tag{32}$$

$$f_x = -x_0 - \frac{\omega}{2} \sum_{j=1}^{k} C_j \frac{\sinh j\omega a}{\cosh j\omega a - \cos j\omega \eta}. \tag{33}$$

2. η_n were determined to satisfy Eq. (28) with C_j, x_0 obtained in the process 1. Namely, η_n were determined to minimize Eq. (34) with the complex method.

$$g(\eta_n) = \left[y_n - \left\{ \eta_n + \frac{\omega}{2} \sum_{j=1}^{k} C_j \frac{\sin j\omega \eta_n}{\cosh j\omega a - \cos j\omega \eta_n} \right\} \right]. \tag{34}$$

3. Residual $\|r\|_2$ was calculated from C_j, x_0 and η_n determined above processes.

$$\|r\|_2 = \|\mathbf{x} - \mathbf{FC}\| = h(a), \tag{35}$$

   a was determined to minimize $h(a)$.
4. $\|r\|_2$ were calculated under various a values. When $\|r\|_2$ was minimum, C_j, x_0 and a were determined as the solution.

The authors found that the above process cannot give appropriate coefficients for some surface profiles. So further study is required to use this elastic solution widely.

5. Prediction of fatigue limit reliability of complex surface

Nomenclature

$F(\sigma)$ cumulative probability function
$f(\sigma)$ probability density function
Other symbols are defined in Nomenclature in Section 3.

5.1. Prediction of fatigue limit

Figure 10 shows a typical relation between notch root radius and fatigue limit. σ_{w1} and σ_{w2} are called the fatigue crack initiation limit and the fatigue crack propagation limit, respectively. In other words, σ_{w1} and σ_{w2} is the fatigue strength of crack initiation from notch root and the fatigue strength of crack. Therefore, σ_{w1} and σ_{w2} can be predicted by the notch model and the crack model in Figure 6, respectively. Then fatigue limit of an arbitrary notched specimen σ_w can be expressed with σ_{w1} and σ_{w2} as follows.

$$\sigma_w = \max(\sigma_{w1}, \sigma_{w2}). \tag{36}$$

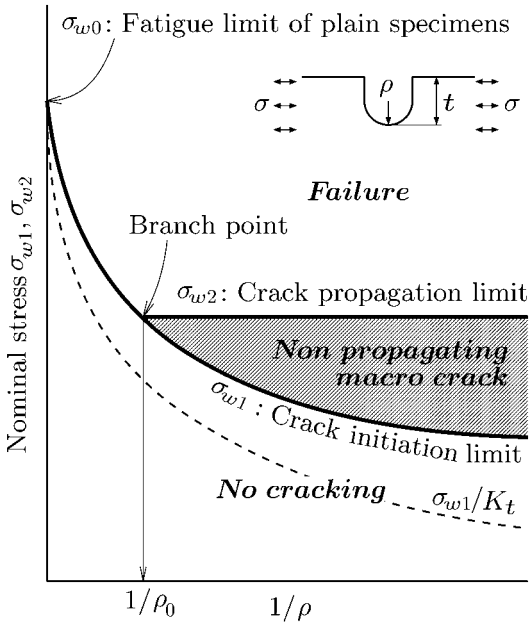

Figure 10. Relation between σ_{w1}, σ_{w2} and ρ ($t =$ const.).

Table 3. Required parameters for fatigue limit evaluation.

	Linear notch mechanics	$\sqrt{\text{area}}$ parameter model
Mechanical severity	Notch root radius ρ, stress concentration factor K_t	Equivalent crack length $\sqrt{\text{area}}$
Material constants	Maximum stress $K_t\sigma_{w1}$ for fatigue crack initiation limit of each ρ	Vickers hardness H_V

It is well known that the linear notch mechanics (Nisitani, 1994) is effective on the evaluation of the fatigue crack initiation limit. While it is well known that the $\sqrt{\text{area}}$ parameter model (Murakami, 2002) is effective on the evaluation of the fatigue crack propagation limit. Table 3 shows necessary parameters for the linear notch mechanics and the $\sqrt{\text{area}}$ parameter model. σ_{w1} of steel can be obtained from the following equation in the case of the stress ratio $R = -1$ (Miyazaki et al., 2004).

$$\sigma_{w1} = \frac{\sigma_{w0}}{K_t}\sqrt{1 + \frac{230}{H_V^{1.46}\rho}}. \tag{37}$$

The unit of notch root radius, ρ, is mm. On the other hand, σ_{w2} can be obtained from Eq. (2).

5.2. Prediction of fatigue limit reliability

Many roughness can be simulated with the method described in Section 2, and σ_{w1} and σ_{w2} of each simulated roughness can be estimated. Consequently, the cumulative probability functions of σ_{w1} and σ_{w2}, $F_1(\sigma_{w1})$ and $F_2(\sigma_{w2})$, can be obtained by the

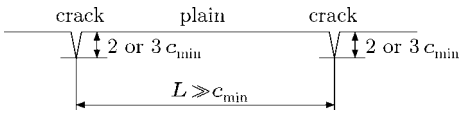

Figure 11. An invalid case of the present method application.

mean rank method with simulated σ_{w1} and σ_{w2} data. Finally, a cumulative probability function and a probability density function of a specimen with surface roughness, $F(\sigma_w)$ and $f(\sigma_w)$, are obtained as follows from Eq. (36):

$$F(\sigma_w) = F_1(\sigma_w)F_2(\sigma_w), \qquad f(\sigma_w) = \frac{\mathrm{d}F(\sigma_w)}{\mathrm{d}\sigma_w}. \tag{38}$$

6. Limitation of the present prediction method

The effective profile on fatigue limit obtained by the process of Section 3 has following problems:

1. larger σ_{w1} may be estimated, because ρ is underestimated by cutting off high order wave elements in the Fourier series;
2. larger σ_{w2} may be estimated, because t and c are underestimated by cutting off high order wave elements in the Fourier series.

Figure 11 is one of examples that the present prediction gives a wrong result; The figure shows a half infinite plate with periodical cracks which length are two or three times longer than $c_{\min}$. The space between two adjacent cracks is much larger than $c_{\min}$.

In the case of a roughness profile in Figure 11, like scratch cracks, will be regarded as a plain surface by the coarse graining of Eq. (4) This result will be brought by the characteristic of Fourier series. In this case, ρ, t and c will be underestimated. Therefore, as the present method gives a dangerous result to a problem like Figure 11, the present method should not be applied to such problems.

7. Application to axisymmetric surface roughness

7.1. Fatigue test

Rotating bending fatigue tests were carried out to examine the present prediction method. Material used is 0.1% carbon steel. Tables 4 and 5 show the chemical composition and mechanical properties respectively.

Figure 12 shows the specimen configuration. The surface roughness was machined under the condition of 0.15 mm depth of cut and manual feed by a turning machine. The specimens were annealed at 600 ° C for 2 h in vacuum after machined. The residual stress on the surface was 1.4 MPa according to a X-ray residual stress measure instrument. So the influence of the residual stress was neglected. Figure 13 shows a roughness profile measured with a stylus instrument, Kosaka Laboratory SE1700. This figure is a typical one in 11 measured curves.

On fatigue test, an Ono-type rotating bending machine was used at 2400 rpm. Stress is defined as the nominal stress defined at the minimum section. Figure 14

Table 4. Chemical composition of 0.1% carbon steel (wt.%).

C	Si	Mn	P	S	Cu	Al	Ni+Cr
0.13	0.22	0.39	0.013	0.022	0.09	0.010	0.10

Table 5. Mechanical properties of 0.1% carbon steel.

σ_{SL} (MPa)	σ_B (MPa)	σ_T (MPa)	ϕ (%)	H_V (kgf/mm^2)	σ_{w0} (MPa)
203	302	771	67.7	120	190

σ_{SL} : Lower yield stress.
σ_B : Ultimate tensile stress.
σ_T : True fracture stress.
ϕ : Reduction of area.
H_V : Vickers hardness.
σ_{w0} : Fatigue limit of electro-polished specimen.

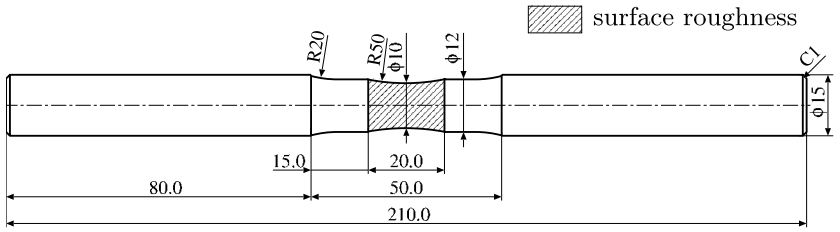

Figure 12. Shape and dimensions of specimen [mm].

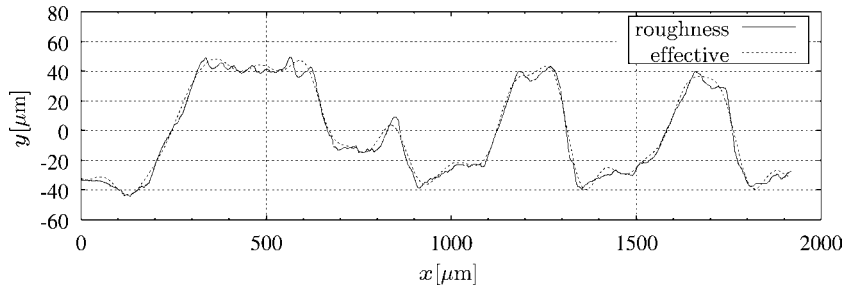

Figure 13. A measured roughness and the effective profile on fatigue limit.

shows S–N curve of the specimens with a roughness shown in Figure 13. The fatigue limit was 165 MPa.

7.2. Comparison between fatigue test and reliability prediction

Figure 13 shows a measured roughness profile and the effective profile on fatigue limit obtained with Eq. (4) While Figure 15 shows the stress concentration along the effective profile on fatigue limit of Figure 13 with the analysis method described in Section 4. Figure 16 shows one of simulated profiles from the spectrum of Figure 13 with the procedure in Section 2 and the effective profile on fatigue limit with the

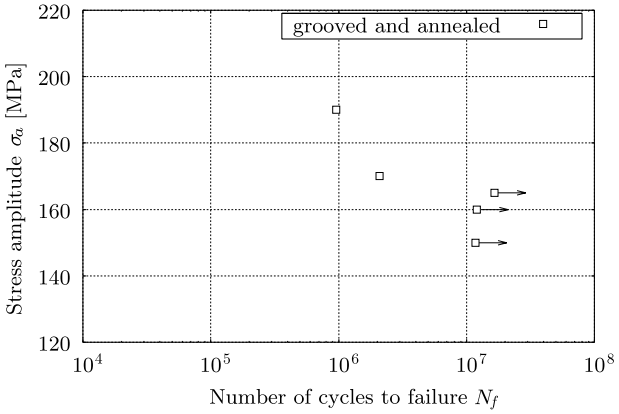

Figure 14. S–N curve of grooved and annealed specimen.

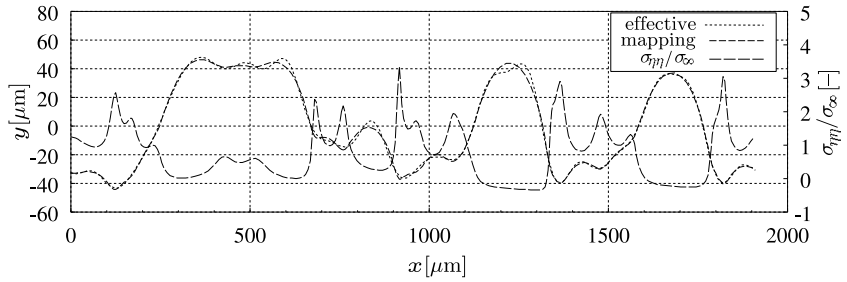

Figure 15. The effective profile on fatigue limit and the normal stress distribution along surface of Figure 13.

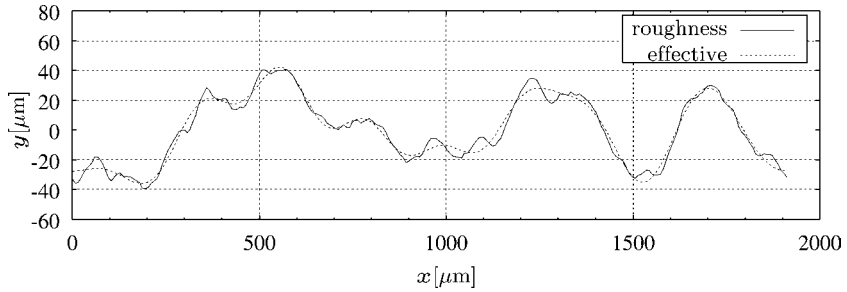

Figure 16. A simulated roughness and the effective profile on fatigue limit.

procedure in Section 3. Figure 17 shows the stress concentration along the effective profile of Figure 16.

It is very difficult to fit the Hirano's conformal mapping to effective profile on fatigue limit completely. The mapping functions tends to have sharp notch root. So the evaluation of stress concentration factor was described as the following procedure:

1. the fitting procedure described in Section 4 was carried out;
2. three of the most deepest vallis were selected and notch root radii of the vallis are calculated for effective profile and mapped function;
3. k, degree of Hirano's mapping function, was degraded to match the notch root radii of the mapping function with those of the effective profiles better;
4. degraded k was used to calculate stress concentrations.

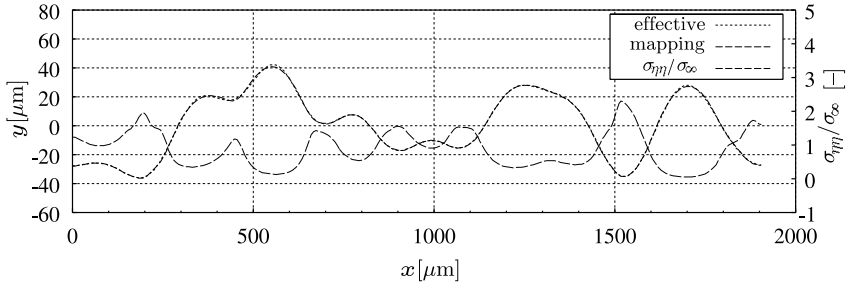

Figure 17. The effective profile on fatigue limit and the normal stress distribution along surface of Figure 16.

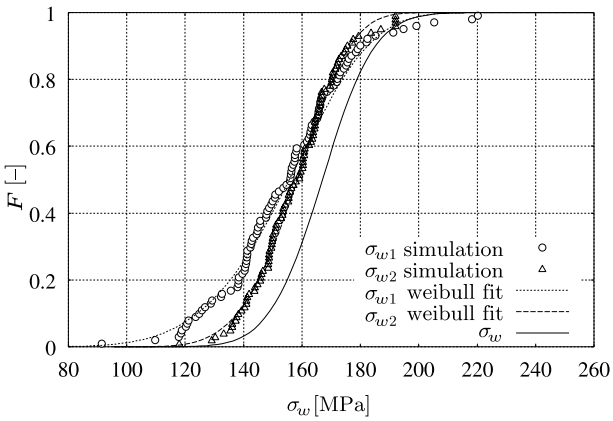

Figure 18. Reliability of fatigue limit.

Then σ_{w1} and σ_{w2} of a profile were determined for the valley with the most high stress concentration in those three vallis. Authors found empirically that this correction gives a little safety-side stress concentration. So it is supposed that the correction can be applied to other type of surface profile. Further study is needed for more accurate calculation.

One hundred curves were simulated from the profile in Figure 13, and σ_{w1} and σ_{w2} of each curve were evaluated. The cumulative probability functions of σ_{w1} and σ_{w2} were obtained with mean rank method. These data were fitted with following 3-parameter Weibull distribution:

$$F(\sigma) = 1 - \exp\left\{-\left(\frac{\sigma - \gamma}{\alpha}\right)^m\right\}. \tag{39}$$

Figure 18 shows $F_1(\sigma_{w1})$, $F_2(\sigma_{w2})$ and $F(\sigma_w)$. Table 6 shows the values of Weibull parameters.

Although the experimental fatigue limit is 165 MPa, this value corresponds to about 45% probability of $F(\sigma)$ and the safety-side fatigue limit is given by the present method. In order to confirm the accuracy of the Weibull probability, a much larger number of test results are needed. But accuracy of the fitting of the mapping function is not enough to discuss this point. So the discussion is restricted within a mean value.

Table 6. Weibull parameters of simulated reliability.

	m (−)	α (MPa)	γ (MPa)
σ_{w1}	5.26	112	51.2
σ_{w2}	4.75	68.0	95.5

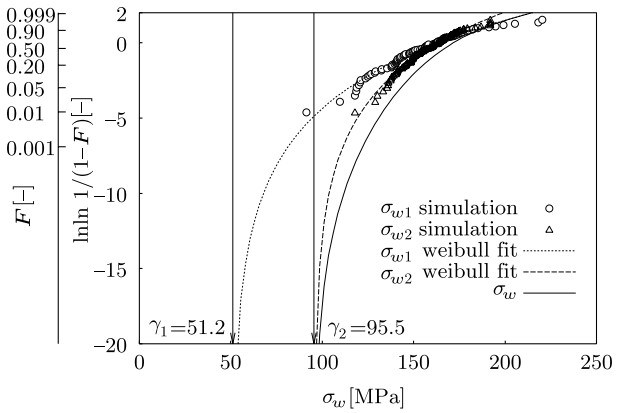

Figure 19. Weibull plot of σ_{w1} and σ_{w2}.

Finally, Figure 19 shows the data on Weibull probability paper. As γ_2 value in $F_2(\sigma_{w2})$ means the lower limit of σ_w of this specimen, the fatigue limit in design may be 95.5 MPa for the specimen with the surface like Figure 13.

8. Conclusion

1. A method to simulate stochastic irregularity has been proposed.
2. The effective profile on fatigue limit evaluation has been derived from the coarse graining.
3. The equivalent notch depth has been defined.
4. An infinite plate with a complex surface profile under uniform tension has been analyzed to develop the Hirano's mapping function. The solution can be applied to surface roughness.
5. A prediction method for fatigue limit reliability of material with complex surface has been proposed.

Appendix A. Derivation of Equations (10) and (11)

A general forms of a periodic stress field concerned with y-direction is expressed by the following equations:

$$\sigma_{xx}+\sigma_{yy}=2\{\Omega'(z)+\overline{\Omega'(z)}\}, \tag{A1}$$

$$\sigma_{yy}-i\sigma_{xy}=\Omega'(z)+\overline{\Omega'(z)}+z\overline{\Omega''(z)}+\overline{\omega'(z)}, \tag{A2}$$

$$\Omega(z)=\Omega_0(z)+f_1(z), \tag{A3}$$

$$\omega(z)=z\Omega_0'(z)+\omega_0(z)+f_2(z). \tag{A4}$$

Here, $\Omega(z)$, $\omega(z)$, $\Omega_0(z)$, $\omega_0(z)$, $f_1(z)$ and $f_2(z)$ are complex stress functions. Moreover, $f_1(z)$ and $f_2(z)$ must be periodic functions concerned with y.

Expressions of Eqs. (A3) and (A4) on mapped ζ plane is represented as $\Omega(m(\zeta))=\Omega(\zeta)$ and $\omega(m(\zeta))=\omega(\zeta)$ for $z=m(\zeta)$.

$$\Omega(\zeta)=\Omega_0(\zeta)+f_1(\zeta), \tag{A5}$$

$$\omega(\zeta)=\frac{m(\zeta)}{m'(\zeta)}\Omega_0'(z)+\omega_0(z)+\frac{m(\zeta)}{m'(\zeta)}f_1'(\zeta)+f_2(\zeta). \tag{A6}$$

Equations (10) and (11) are obtained to substitute $\Phi_0(\zeta)=\Omega_0'(\zeta)/m'(\zeta)$, $\phi_0(\zeta)=\omega_0'(\zeta)/m'(\zeta)$, $g_1(\zeta)=f_1'(\zeta)/m'(\zeta)$ and $g_2(\zeta)=f_2'(\zeta)/m'(\zeta)$ for Eqs. (A5) and (A6).

References

Andrews, S. and Sehitoglu, H. (2000). A computer model for fatigue crack growth from rough surfaces. *International Journal of Fatigue* **22**, 619–630.

El-Helieby, S.O.A. and Rowe, G.W. (1980). Influence of surface roughness and residual stress on fatigue life of ground steel components. *Metals Technology* **7**(6), 221–225.

England, A.H. (1971). *Complex Variable Methods in Elasticity*. John Wiley & Sons, London, UK.

Garwood, M.F., Zurburg, H.H. and Erickson, M.A. (1951). Correlation of laboratory tests and service performancs. In: *Interpretation of Tests and Correlation with Service*. ASM, Philadelphia, 1–77.

Hirano, F. (1950). Study on the shape factor of 2D elastic body. *Journal of the Japan Society of Mechanical Engineers* **16**(55), 52–58. in Japanese.

Inglis, C.E. (1913). Stress in a plate due to the presence of cracks and sharp corners. *Transactions of the Institution of Naval Architectures* **55**, 219–230.

Murakami, Y. (1985). Analysis of stress intensity factors of modes I, II and III for inclined surface cracks of arbitrary shape. *Engineering Fracture Mechanics* **22**(1), 101–114.

Murakami, Y. (2002). *Metal Fatigue : Effects of Small Defects and Nonmetallic Inclusions*. Elsevier Science Ltd.

Nisitani, H. (1994). Linear notch mechanics as an extension of linear fracture mechanics, In: *Computational and Experimental Fracture Mechanics (Topics in Engineering vol.16)*. Computational Mechanics Publications, Southhampton UK and Boston USA, 187–211.

Siebel, E. and Gaier, M. (1957). Influence of surface roughness on the fatigue strength of steels and non-ferrous alloys. *Engineers Digest* **18**, 109–112. Translation from VDI-Zeitschrift, vol. 98, 1956, 1715–1723.

Sinclair, G.M., Corten, H.T. and Dolan, T.J. (1957). Effect of surface finish on the fatigue strength of titanium alloys RC 130B and Ti 140A. *Transactions ASME* **79**(1), 89–96.

Taylor, D. and Clancy, O.M. (1991). The fatigue performance of machined surfaces. *Fatigue and Fracture of Engineering Materials and Structures* **14**(2/3), 329–336.